Commun. Fac. Sci. Univ. Ank. Series B
V.53 (1). pp. 1- 14 (2007)

CHANGES IN CRYSTAL STRUCTURE, THERMAL BEHAVIOR AND SURFACE AREA OF A BENTONITE BY ACID ACTIVATION

M. ÖNAL

Ankara University, Faculty of Science, Department of Chemistry, Tandoğan, 06100 Ankara, Turkey.
(onal@science.ankara.edu.tr)

(Received April 6 , 2007; Accepted May 3, 2007)

ABSTRACT

A commercial calcium bentonite (CaB) taken from Kütahya, Turkey, was activated with H_2SO_4 by wet method at 97°C for 6h. The H_2SO_4% by mass was changed from zero to 70 in the dry bentonite-acid mixture. X-ray diffraction (XRD) analysis shows that the crystallinity of calcium smectite (CaS) in the CaB with the 65% by mass decreases greatly by the acid activation. Dehydration mechanism of the CaS changes by the activation. Maximum rate temperatures for dehydroxylation and decrystallization of the CaS decrease depending on the decreasing of the crystallinity. The specific surface area (*S*) obtained from the nitrogen adsorption data with the different methods were compared and discussed according to the H_2SO_4%. The arithmetic average of the specific surface areas, $\langle S \rangle$, increases from $44 m^2 g^{-1}$ to its maximum value of $136 m^2 g^{-1}$ by the activation at 40% H_2SO_4 and then reaches to $73 m^2 g^{-1}$ at 70% H_2SO_4.

KEYWORDS: Acid activation; bentonite; crystallinity; smectite; surface area; thermal effect

INTRODUCTION

Smectites are major clay minerals in bentonites. An ideal smectite is a 2:1 layer clay mineral and has two silica tetrahedral (T) sheets bonded to a central alumina octahedral (O) sheet [1,2]. The isomorphic substitution in the octahedral sheets of Fe^{2+} and Mg^{2+} for Al^{3+}, and in tetrahedral sheets of Al^{3+} for Si^{4+} cause a net negative charge on the 2:1 (TOT) layers. This negative charge is balanced by the exchangeable cations such as Na^+ and Ca^{2+} located between the layers and around the edges. It is called sodium smectite (NaS) or calcium smectite (CaS) according to the abundance of one of these cations. Bentonite powders or rocks are mainly formed by the agglomeration of the 2:1 layers. These agglomerates can disperse spontaneously below 2μm in aqueous suspension after staying for a long time. The air dried natural NaS and CaS have respectively one water layer and two water layers between the 2:1 layers, and their basal spacing, *d*(001), are 1.26nm, and 1.54nm, according to X-ray diffraction (XRD) patterns [3,4]. Commercial bentonites

generally contain either Na-montmorillonite (NaM) or Ca-montmorillonite (CaM) as smectite mineral [5,6].

The total surface area of one gram bentonite is defined as specific surface area (S/m^2g^{-1}) as same as by other porous materials. The extent of the surface area affects greatly some industrial uses of bentonites such as adsorbent, desiccant, catalyst, bleaching earth, drilling mud, pharmaceutical, paper, cosmetic, and paint [7-11]. The acid activation is changed the crystallinity, thermal behavior, and surface area of bentonites by exchange between protons and interlayer cations, aggregation of particles, elimination of several nonclay mineral impurities, and removal of metal cations from some octahedral and tetrahedral positions [12-21]. Surface area of a bentonite can be more increased by the exchange of the natural interlayer cations with some larger organic cations and inorganic polycations. Thus, organoclays and pillared clays are synthesized [22-26].

The specific surface area of natural, acid activated, and cation-exchanged bentonites has been determined by the measuring of monolayer adsorption capacities of some particular polar and apolar molecules [13,27-33]. Polar molecules such as water, glycerol, amines, ethylene glycol, and ethylene glycol monoethyl ether can penetrate the interlayer regions of smectites, whereas apolar molecules such as nitrogen, argon, and ethane can not [34-36]. Thus, specific area of a bentonite determined by using polar molecules is larger than by apolar molecules [37-41]. Nitrogen gas having apolar molecules with the cross-sectional area of $0.162nm^2$ has been generally used for the specific surface area determination of the bentonites as well as other porous materials [42,43]. Several methods have been purposed for the determination of specific surface area from the nitrogen adsorption data at liquid nitrogen temperature [44-46]. Therefore, the aim of this study the effect of H_2SO_4 activation on the crystallinity, thermal behavior, and specific surface area determined with different methods by using nitrogen adsorption data.

MATERIALS AND METHOD

A calcium bentonite (CaB) with the white color taken from Kütahya bed, Turkey, was used in this study. Some physicochemical properties of the soda, acid and heat treated samples of this bentonite were previously examined [47-49]. The bulk chemical analysis (as mass %of metal oxides) of the CaB dried at 105°C for 4h is: SiO_2, 72.08; Al_2O_3, 14.77; Fe_2O_3, 0.80; TiO_2, 0.08; MgO, 1.63; CaO, 2.15; Na_2O, 0.43; K_2O, 1.05; and loss on ignition (LOI), 6.71. The CaB contain beside calcium smectite (CaS) and illite (I) as major and minor clay minerals respectively and also opal-CT (OCT) with the great amount and other nonclay impurities. The mass % of CaS, OCT and other impurities in the CaB was estimated as 65%, 30% and 5%, respectively by evaluating the chemical analysis [50].

The prepare porous solids having different specific surface areas the CaB samples dried at 105°C for 4h were activated with H_2SO_4 used various dosages. Samples, each having a mass 20g taken from the dried CaB were treated with H_2SO_4 by wet method. Each sample was mixed with H_2SO_4 solution of 400mL and obtained suspension heated at 97°C for 6h in shaking water bad. The concentration of H_2SO_4 solution was changed corresponding to the increasing of mass % of H_2SO_4 in the dried bentonite-acid mixture in the interval between zero and 70. After acid activation, each suspension was filtered under vacuum and the precipitate was washed with distilled water until free SO_4^{2-} ions. The acid treated samples were air dried and stored in the plastic bottles closed tightly.

The X-ray diffraction (XRD) patterns of the original and H_2SO_4 activated bentonites were obtained from random mounts using a Rikagu D-Max 2200 powder diffractometer with CuK_α radiation and a Ni filter. The differential thermal analysis (DTA) curve for original and acid activated samples was recorded using a Shimadzu Apparatus (DTG-60H). Approximately 20mg of sample was placed in a platinum crucible on the pan of the microbalance and was heated in the range of 25-1000°C using α-Al_2O_3 as an inert material. Analysis was performed under flowing nitrogen with the rate of 100mL min^{-1} using heating rate of 10°C min^{-1}. The adsorption isotherm of N_2 at liquid N_2 temperature on each acid activated sample was determined by a volumetric adsorption instrument of pyrex glass connected to high vacuum [51].

RESULTS AND DISCUSSION

Change in crystallinity and thermal behavior

The XRD patterns of the original and acid activated samples were examined, and representative ones, are shown in Fig. 1. The characteristic reflections for CaS and OCT are seen at 1.538nm and 0.406nm, respectively. Although the intensity of the 001 XRD reflections for CaS decreases, the 101 XRD reflection for OCT remains unchanged by acid activation. This indicates that the paracrystallinity of OCT is not affected from the H_2SO_4 activation. The crystallinity of CaS decreases continuously by increase in H_2SO_4. This increasing is affected some of the physicochemical properties of the bentonite.

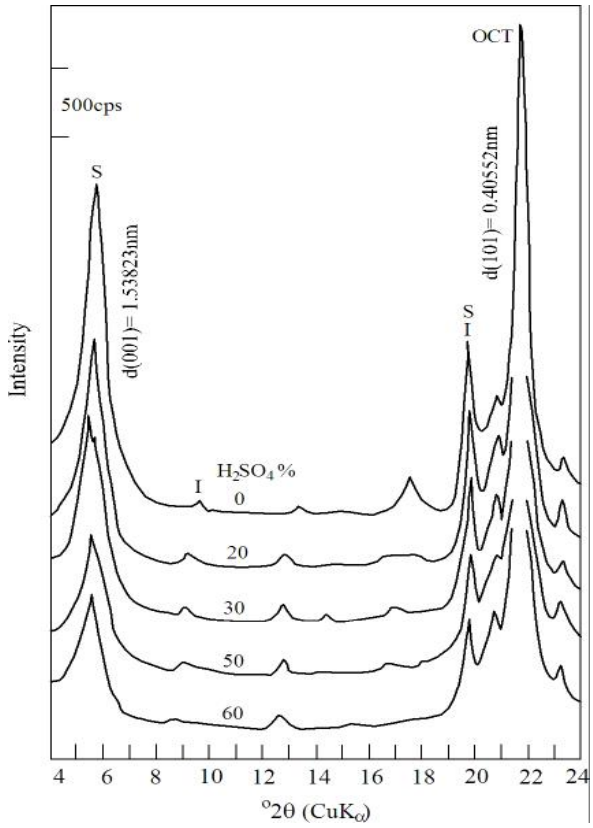

Fig. 1. The X-ray diffraction (XRD) patterns (S: smectite, I: illite, OCT: opal-CT)

The DTA curves of the original and acid activated samples were examined, representative ones, are given in Fig. 2. Two endothermic changes and one exothermic change are seen in the DTA curves. The maximum rate temperature of these changes is indicated on the DTA curves in Fig. 2. The first and dominant endothermic change for the air dried original samples is due to the dehydration of interparticle water, adsorbed water and interlayer water. The peak corresponding to this change for the original bentonite is twin. The change with the maximum rate temperature at 150^{o}C corresponding to the first twin is originated from the

dehydration of interparticle water. The change with the maximum rate temperature at 220°C corresponding to the second twin shows the dehydration of the adsorbed water and interparticle water. The twin peak for dehydration disappears after the acid activation. However, dehydration temperatures for interparticle water, adsorbed water and interlayer water in the bentonite before or after the acid activation can not be strictly distinguished. The second endothermic change between 600 and 800°C is due to the dehydroxylation of the bentonite. The maximum rate temperature for the dehydroxylation decreases from 770 to 720°C by the acid activation, as seen in Fig. 2. The exothermic change between 950 and 1050°C is due to the decrystallization of the CaS. The maximum rate temperature for the decrystallization also reduces from 1025 to 985°C, by the acid activation. This result shows that the H_2SO_4 activation decrease the crystallinity of the CaS.

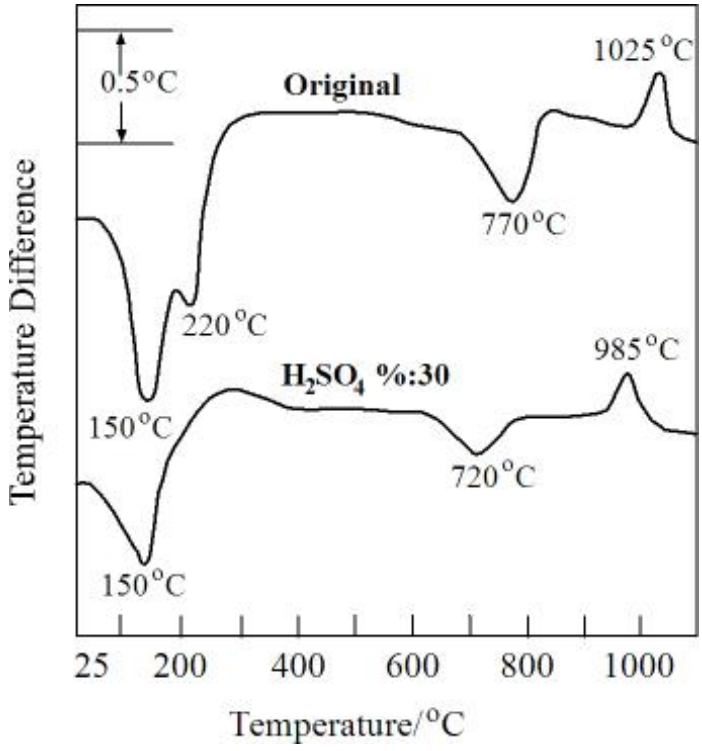

Fig. 2. The differential thermal analysis (DTA) curves

Adsorption isotherms

The adsorption isotherms of N_2 at liquid N_2 temperature on the natural and some acid activated bentonite powders are given in Fig. 3. Here, p is the pressure in equilibrium with the adsorbent, p_o is the pressure in equilibrium with liquid nitrogen, $p/p_o \equiv x$ is the relative adsorption equilibrium pressure, and n/molg^{-1} is the adsorption capacity. The isotherms of all samples are similar to Type II according to Brunauer classification [52]. The increases in adsorption capacity at low and high relative adsorption equilibrium pressures are due to the adsorption in microspores and mesopores respectively. Thus, natural and acid activated bentonite samples are micro-and mesoporous solids. The shapes of the isotherms show that the adsorptions on the samples are multimolecular and capillary condensation occurs. Several equations have been derived for the examination of the adsorption isotherms and determination specific surface area of adsorbents [45]. Some of those including Langmuir, and Dubinin equations valid only for the adsorption on the microporous solids can not be used for the determination of specific surface area of the investigated micro-and mesoporous bentonite samples [46]. The evaluations of the other adsorption isotherm equations in the methods derived for specific surface area determination are given as follows.

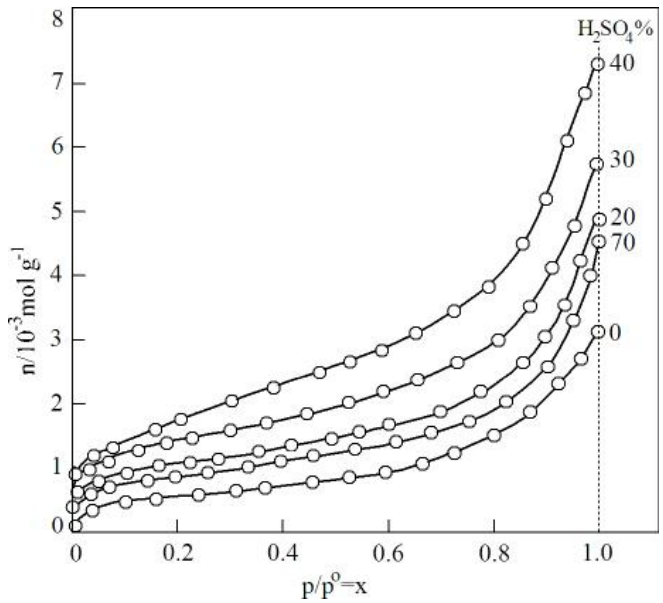

Fig. 3. The nitrogen adsorption and desorption isoterms at liquid nitrogen temperatures

The Brunauer, Emmett, and Teller (BET) method

The plots drawn in $0.05<x<0.35$ interval according to the BET equation derived for multimolecular adsorption and expressed in the linear form;

$$x/n(1-x) = 1/n_m c + [(c-1)/n_m c]\, x, \qquad (1)$$

are given in Fig. 4 [53]. Here, n_m/molg^{-1} is the monomolecular adsorption capacity and c is a constant related to the heat of adsorption. Each BET plot is a straight line with the zero intercept. If the intercept is zero, and that c is sufficiently large, c-1 reaches to c, and the slope may be taken as $1/n_m$. The n_m value for each sample was taken equal to the reciprocal of slope of the BET straight line. The specific surface areas were calculated from the relation.

$$S\ (\mathrm{m^2 g^{-1}}) = n_m\ (\mathrm{molg^{-1}})\ L\ (\mathrm{mol^{-1}})\ \sigma\ (\mathrm{m^2}) \qquad (2)$$

where, $L = 6.02\mathrm{x}10^{23}\mathrm{mol}^{-1}$ is the Avogadro constant and $\sigma = 16.2\mathrm{x}10^{-20}\mathrm{m}^2$ is the average area occupied by each N_2 molecule in the completed monolayer. The calculated specific surface areas are given in Table 1.

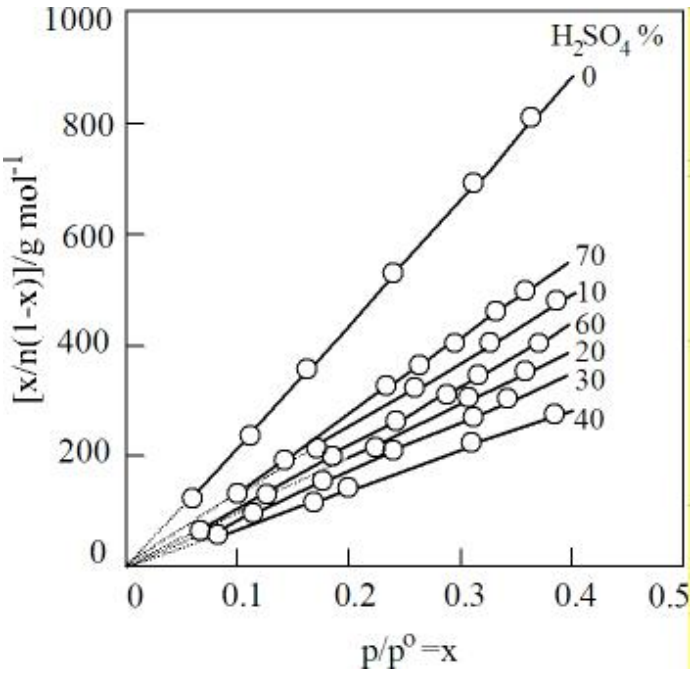

Fig. 4. The Brunauer, Emmett, and Teller (BET) plots

The Lippens and de Boer method (LB)

The adsorption capacity (n/molg^{-1}) at each x was converted to the liquid nitrogen volumes (V/cm^{3}g^{-1}) by using the relation

$$(V/\mathrm{cm^3g^{-1}}) = (34.65\mathrm{cm^3mol^{-1}})\ n\ (\mathrm{molg^{-1}}) \quad (3)$$

where, 34.65cm^{3}mol^{-1} is the molar volume of the liquid nitrogen. The standard multilayer thickness (t/nm) at each x corresponding to V was read from the universal t-curve (t versus x) purposed by Lippens and de Boer [54]. All experimental isotherms are transformed into t-plots as V-t graphs and given in Fig. 5. As seen in this figure, the straight lines were obtained from the extrapolations of the t-plots to t = 0 value. The slopes (V/t) of each straight line were calculated. The specific surface areas were calculated by using the slopes in the equation derived by Lippens and de Boer

$$S\ (\mathrm{m^2g^{-1}}) = 997\ V\ (\mathrm{cm^3g^{-1}})/t\ (\mathrm{nm}) \quad (4)$$

where, 997 is a conversion factor for units. The results are given in Table 1.

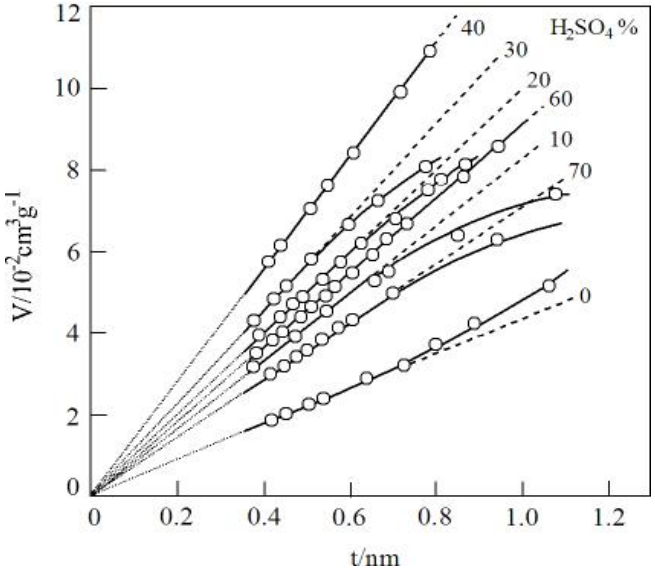

Fig. 5. The Lippens and de Boer (LB) plots

The Sing (α_s) method

The convert the standard nitrogen adsorption data for any test material into an alternative dimensionless form, a non-porous hydroxylated silica was selected as the standard adsorbent [45,46]. The specific surface area, and the adsorption capacity at a pre-selected normalized adsorption equilibrium pressure $p/p_o \equiv x = 0.4$ of the standard adsorbent were measured exactly as S_s=154m^{2}g^{-1} and $n_{0.4}$ = 2.387x10^{-3} molg^{-1} respectively for the adsorption of nitrogen at the liquid nitrogen temperature. The relative adsorption capacities for the standard adsorbent ($\alpha_s = n_s/n_{0.4}$) and test material ($\alpha = n/n_{0.4}$) were calculated at each x. The adsorption isotherm (n-x) for the test material and the α_s-curve (α_s-x) for the standard adsorbent were drawn. The n-α_s plot for each sample was drawn by evaluation of the n-x and α_s-x curves, and representative ones, are given in Fig. 6. The slope of each straight line gives the n/α_s ratio. By an assumption the equality of the S/S_s and α/α_s ratios a relation can be derived as below,

$$S/S_s = \alpha/\alpha_s = (n/n_{0.4})/\ (\ n_s/n_{0.4}) \quad (5)$$

$$S(\mathrm{m^2g^{-1}}) = (6.45\mathrm{x}10^4\mathrm{m^2g^{-1}})\ n\ (\mathrm{molg^{-1}})\ /\alpha_s \quad (6)$$

The specific surface area (S) for each powder was calculated from the last equation by using the corresponding slop (n/α_s), and given in Table 1.

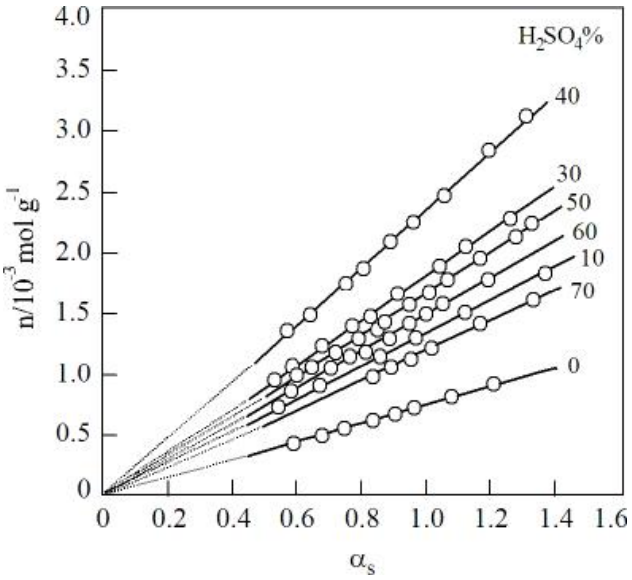

Fig. 6. The Sing (α_s) plots

The Harkins and Jura (HJ) method

The adsorption capacity (n/molg^{-1}) at each x was converted to the nitrogen gas volumes at 273K and 1atm by using the relation

V(cm^{3}g^{-1}) = (22400 cm^{3}g^{-1}) n (molg^{-1}) (7)

where, 22400 cm^{3}g^{-1} is the molar volume of the gas nitrogen at the normal conditions. The plots drawn according to the Harkins and Jura equation derived thermodynamically below

log$x$ = B-C/v^2 (8)

are given in Fig. 7 [55,56]. Here, B and C are the HJ-constants. The specific surface areas were calculated by using the C constant in the relation of

S(m^{2}g^{-1}) = 4.06 $C^{1/2}$, (9)

derived for N_2 adsorption. The HJ-surface areas are given in Table 1.

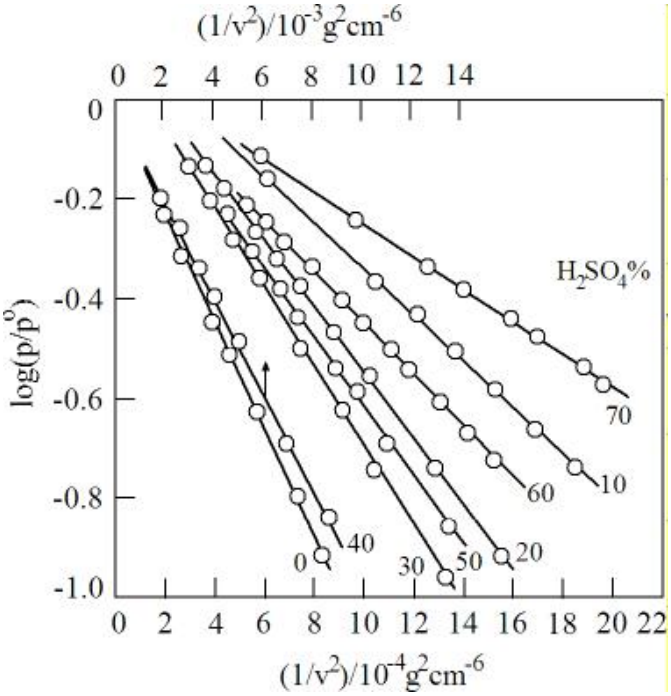

Fig. 7. The Harkins and Jura (HJ) plots

Comparison of the specific surface areas

The BET, LB, α_s, and HJ surface areas seen in Table 1 agree well each other. The arithmetic average of the surface area, <*S*>, is also given Table 1. The variation of the <*S*> with the H_2SO_4% is shown in Fig. 8. The <*S*> value increases from $44 m^2 g^{-1}$ to its maximum of $136 m^2 g^{-1}$ at 40% H_2SO_4 and then decreases to $73 m^2 g^{-1}$ at 70% H_2SO_4.

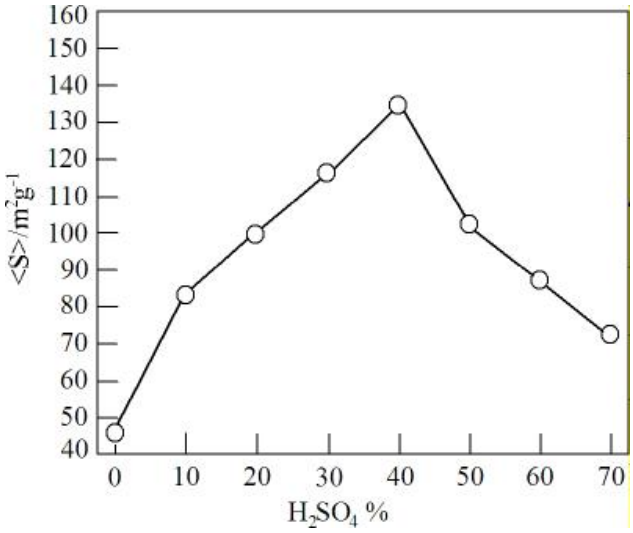

Fig. 8. The variation of the average specific surface area (<*S*>) with the H_2SO_4%

CONCLUSION

In the bentonite, the crystallinity of the CaS decreases continuously with increasing H_2SO_4% by acid activation, while the paracrystallinity of the OCT does not affect. The exchange of interlayer cation with proton by acid activation reduces the dehydroxylation and decrystallization temperatures. The specific surface areas calculated with different methods are agreed well with the value obtained from the standard BET method. The surface area increases three fold of the initial value $44 m^2 g^{-1}$ with the H_2SO_4 activation. The acid activated bentonite samples with the high surface area can be used as adsorbents, bleaching earth, filters, catalysts, and catalyst support.

Table 1 The specific surface areas of the H_2SO_4 activated bentonite samples obtained from different samples by using nitrogen adsorption data

	S /m^2g^{-1}				
H_2SO_4%	BET	LB	α_s	HJ	<S>
0	43	44	45	43	44
10	82	83	84	88	84
20	96	96	103	105	100
30	123	114	116	115	117
40	134	137	148	126	136
50	101	100	103	108	103
60	91	91	97	92	93
70	70	71	77	74	73

ASİT AKTİVASYONU SIRASINDA BİR BENTONİTİN KRİSTAL YAPISI, TERMAL DAVRANIŞI VE YÜZEY ALANINDAKİ DEĞİŞMELER

ÖZET

Kütahya (Türkiye) bölgesinden alınan bir ticari kalsiyum bentonit (CaB) H_2SO_4 ile yaş yöntem uyarınca 97ºC'da 6 saat aktiflenmiştir. CaB içinde kütlesel olarak %65 oranında bulunan kalsiyum smektite (CaS) ilişkin kristalliğin asit aktivasyonu ile büyük ölçüde düştüğü X-ışınları difraksiyonu (XRD) ile belirlenmiştir. Bunun yanında, CaB içinde kütlesel olarak %30 oranında bulunan opal-CT'nin yarı kristalliğinin asit aktivasyonundan etkilenmediği gözlenmiştir. CaS'in dehidratasyon mekanizması asit aktivasyonu ile değişmektedir. CaS'in dehidroksilasyonu ve dekristalizasyonu için maksimum hız sıcaklıkları kristalliğin düşmesine bağlı olarak değişmektedir. Brunauer-Emmett- Teller (BET), Lippens-de Boer (LB), Sing (α_s) ve Harkins- Jura (HJ) yöntemleri uyarınca azotun adsorpsiyon verilerinden hesaplanan özgül yüzey alanlarının (S) birbiri ile uyumu ve H_2SO_4 yüzdesi ile değişimi tartışılmıştır. Özgül yüzey alanlarının <S> aritmetik ortalamasının H_2SO_4 yüzdesi ile 44 m^2g^{-1}'den itibaren artarak H_2SO_4 yüzdesi 40 olduğunda 136 m^2g^{-1} değerine ulaştığı ve daha sonra bu yüzde 70'e yükseldiğinde 73 m^2g^{-1} değerine azaldığı belirlenmiştir.

ACKNOWLEDGEMENT

The author thank the Scientific Research Council of Ankara University, Turkey supporting this study under a Project No: 2003.07.05.082.

REFERENCES

1. Grim, R.E. *Clay Miner.*, 2nd ed., McGraw-Hill, New York, 1968.
2. Murray, H.H. *Appl. Clay Sci.*, 1991, 5, 379-395.
3. Moore, D.M.; Reynolds, Jr., R.C. *X-Ray Diffraction and the Identification and Analysis of Clay Minerals*, 2nd ed., Oxford University Press, Oxford, 1997.
4. Murray, H.H. *Clay Miner.*, 1999, 34, 39-49.
5. Grim, R.E.; Güven, N. *Bentonites-Geology, Mineralogy, Properties and Uses (Developments in Sedimentology, 24)*, Elsevier, New York, 1978.
6. O'Driscoll, M. *Ind. Miner.*, 1988, 43-67.
7. Chitnis, S.R.; Sharma, M.M. *Reac. Func. Poly.*, 1997, 32, 93-115.
8. Christidis, G.E.; Scott, P.W.; Dunham, A.C. *Appl. Clay Sci.*, 1997, 12, 329-347.
9. Murray, H.H. *Appl. Clay Sci.*, 2000, 17, 207-221.
10. Lin, S-H.; Juang, R-S; Wang, Y-H. *J. Hazar. Mater. B*, 2004, 113, 195-200.
11. Hart, M.P.; Brown, D.R. *J. Mol. Catal. A: Chem.*, 2004, 212, 315-321.
12. Mills, G.A.; Holmes, J.; Cornelius, E.B. *J. Phys. Colloid Chem.*, 1950, 54, 1170-1185.
13. Lopez-Gonzalez, J.D.; Deitz, V. *J. Res. Nat. Bure. Stan.,* 1952, 48, 325-333.
14. Heyding, R.D.; Ironside, R.; Norris, A.R.; Prysiazniuk, R.Y. *Can. J. Chem.*, 1960, 38, 1003-1016.
15. Takáč, I.; Komadel, P.; Müller, D. *Clay Miner.*, 1994, 29, 11-19.
16. Kumar, P.; Jasra, R.V.; Bhat, T.S.G. *Ind. Eng. Chem. Res.*, 1995, 34, 1440-1448.
17. Komadel, P.; Bujdák, J.; Madejová, J.; Šucha, V.; Elsass, F. *Clay Miner.*, 1996, 31, 333-345.
18. Vincente, M.A.; Suárez, M.; López-González, J.D.; Bañares-Muñaz, M.A. *Langmuir*, 1996, 12, 566-572.
19. Jozefaciuk, G.; Bowanko, G. *Clays Clay Miner.*, 2002, 50, 771-783.
20. Komadel, P. *Clay Miner.*, 2003, 38, 127-138.
21. Temuujin, J.; Jadambaa, Ts.; Burmaa, G.; Erdenechimeg, Sh.; Amarsanaa, J.; MacKenzie, K.J.D. *Ceram. Inter.*, 2004, 30, 251-255.
22. Pinnavaia, T.J. *Science*, 1983, 220, 365-371.
23. Adams, J.M. *Appl. Clay Sci.*, 1987, 2, 309-342.
24. Barrer, R.M. *Clays Clay Miner.*, 1989, 37, 385-395.
25. Ge, Z. ; Li, D.; Pinnavaia, T.J. *Micro. Mater.*, 1994, 3, 165-175.
26. Varma, R.S. *Tetrahedron*, 2002, 58, 1235-1255.
27. Paterson, E. *Clay Miner.*, 1977, 12, 1-9.
28. Mikhail, R. SH.; Guindy, N.M.; Hanafi, S., *J. Colloid Interf. Sci.*, 1979, 70, 282-292.
29. Juhász, A.Z. *Colloid. Surf.*, 1990, 49, 41-55.
30. Jovanović, N.; Janaćković, J. *Appl. Clay Sci.*, 1991, 6, 59-68.

31. Rodriquez, M.A.V.; Barrios, M.S.; Gonzalez, J.D.L.; Muñoz, M.A.B. *Clays Clay Miner.*, 1994, 42, 724-730.
32. Christidis, G.E. Greece, *Appl. Clay Sci.*, 1998, 13, 79-98.
33. Mohino, F.; Martin, A.B.; Salerno, P.; Bahamonde, A.; Mendioroz, S. *Appl. Clay Sci.*, 2005, 29, 125-136.
34. Kinter, E.B.; Diamond, S. *Clays Clay Miner.*, 1958, 5, 318-333.
35. Bower C.A. *Soil Sci.*, 1963, 95, 192-195.
36. McNeal, B.L. *Soil Sci.*, 1964, 97, 96-102.
37. Diamond, S.; Kinter, E.B. *Clays Clay Miner.*, 1958, 5, 334-347.
38. Bower, C.A.; Goertzen, J.O. *Soil Sci.* 1959, 87, 289-292.
39. Milford, M.H.; Jackson, M.L. *Science*, 1961, 135, 929-930.
40. Carter, D.L.; Heilman, M.D.; Gonzalez, C.L. *Soil Sci.*, 1965, 100, 356-360.
41. Heilman, M.D.; Carter, D.L.; Gonzalez, C.L. *Soil Sci.*, 1965, 1000, 409-413.
42. McClellan, A.L.; Hornsberger, H.F. *J. Colloid Interf. Sci.* 1967, 23, 577-599.
43. Everett, D.H.; Parfitt, G.D.; Sing, K.S.W.; Wilson, R. *J. Appl. Chem. Biotech.*, 1974, 24, 199-219.
44. Linsen, B.G. *Physical and Chemical Aspects of Adsorbent and Catalysts,* Academic Press, London, 1970.
45. Gregg, S.J.; Sing, K.S.W. *Adsorption, Surface Area and Porosity*, 2nd ed., Academic Press, London, 1982.
46. Rouquerol, F.; Rouquerol, J.; Sing, K. *Adsorption by Powder and Porous Solids,* Academic Press, London, 1999.
47. Yıldız, N.; Sarıkaya, Y.; Çalımlı, A. *Appl.Clay Sci.*, 1999, 14, 319-327.
48. Sarıkaya, Y.; Önal, M.; Baran, B.; Alemdaroğlu, T. *Clays Clay Miner.*, 2000, 48, 557-562.
49. Önal, M.; Sarıkaya, Y.; Alemdaroğlu, T.; Bozdoğan, İ. *Turk.J. Chem.*, 2002, 26, 409-416.
50. Kahraman, S.; Önal, M.; Sarıkaya, Y.; Bozdoğan, İ. *Analytica Chimica Acta*, 2005, 552, 201-206.
51. Sarıkaya, Y.; Aybar, S. *Commun. Fac. Sci., Univ. Ank.,* 1978, 24B, 33-39.
52. Brunauer, S.; Deming, L.S.; Deming, W.E.; Teller, E. *J. Amer. Chem. Soc.,* 1940, 62, 1723-1732.
53. Brunauer, S.; Emmett, P.H.; Teller, E. *J. Amer. Chem. Soc.*, 1938, 60, 308-319.
54. Lippens, B.C.; de Boer, J.H. *J. Catal.*, 1965, 4, 319-323.
55. Harkins, W.D.; Jura, G. *J. Amer. Chem. Soc.*, 1994a, 66, 1362-1366.
56. Harkins, W.D.; Jura, G. *J. Amer. Chem. Soc.*, 1994b, 66, 1366-1373.